Secrecy Offloading Analysis of UAV-assisted NOMA-MEC Incorporating WPT in IoT Networks

Gia-Huy Nguyen
ICT Department
FPT University
Hanoi 10000, Vietnam
huynghe180064@fpt.edu.vn

Anh-Nhat Nguyen
ICT Department
FPT University
Hanoi 10000, Vietnam
nhatna3@fe.edu.vn

Khai Nguyen
ICT Department
FPT University
Hanoi 10000, Vietnam
khainhe176049@fpt.edu.vn

Minh-Sang Nguyen
ICT Department
FPT University
Hanoi 10000, Vietnam
sangnmhe176048@fpt.edu.vn

Tung-Son Ngo
ICT Department
FPT University
Hanoi 10000, Vietnam
sonnt69@fe.edu.vn

Ngoc-Anh Bui
ICT Department
FPT University
Hanoi 10000, Vietnam
anhbn5@fe.edu.vn

Phuong-Chi Le
ICT Department
FPT University
Hanoi 10000, Vietnam
chilp2@fe.edu.vn

Manh-Duc Hoang
ICT Department
FPT University
Hanoi 10000, Vietnam
duchm29@fe.edu.vn

***Abstract*—This article studies the efficiency of secrecy data offloading for an unmanned aerial vehicle (UAV)-assisted nonorthogonal multiple access (NOMA)-integrated mobile-edge computing (MEC) incorporating wireless power transfer (WPT) within an Internet of Things (IoT) network. Specifically, this study assumes UAV to function in dual roles: as a mobile computation platform and as an aerial power-supply station, offering substantial advantageous for resource-constrained edge devices (EDs) in mitigating interference from an passive eavesdropper. To assess the system's secrecy offloading efficacy, the secrecy successful computation probability (SSCP) closed-formed formulation under Nakagami-m fading channel is derived. The theoretical results are conducted with a variety of parameters, thereby validating the precision of our analysis.**

***Index Terms*—unmanned aerial vehicle, nonorthogonal multiple access, wireless power transfer, mobile edge computing.**

I. Introduction

The advent of next generation networks has significantly enhanced connectivity and data interchange propagation, paving the way for the rapid expansion of Internet of Things (IoT) devices [1]–[3]. While these networks are acquired with the capability of delivering high-speed data transfer and extensive coverage, they also introduce inevitable deficiencies, such as network congestion and security vulnerabilities [4], [5].

Nonorthogonal multiple access (NOMA) and physical-layer security (PLS) have offered viable solutions to tackle the incoming challenges [6]. By utilizing the power domains, NOMA facilitates the concurrent data transmission across a multitude of mobile users within identical time resources, thereby promoting the spectral efficiency and user fairness [7]. On the other hand, by exploiting the physical properties of the wireless communication, PLS is capable of safeguarding data confidentiality against hostile attacks or eavesdroppers, thus enhancing the secrecy of NOMA-applied systems [8]. However, the high-speed NOMA services cause substantial energy consumption in mobile devices, which directly contributes to the computation-constrained issue.

Thus, wireless power transfer (WPT) and mobile-edge computing (MEC) have emerged as pivotal technologies [9]. WPT offers a promising solution to the energy demands of IoT networks by enabling the continuous wireless power-supply to mobile devices, reducing the need of battery placements [10]. Furthermore, to address the data computation issue, the key feature of MEC permits the mobile devices to offload computation-intensive tasks to the edge severs [11]. Hence, the network robustness can be enhanced [12].

In addition, current research has increasingly focused on the evaluations of the unmanned aerial vehicle (UAV) in NOMA-MEC systems [13]. The unique features of UAV, including flexible deployments, the establishment of strong Line-of-Sight (LoS) transmissions, extensive coverage over large areas, contribute to the advantages of providing superior communication quality compared to the conventional installations of terrestrial cellular networks.

Driven by the preceding discourses, this study examines an UAV-assisted NOMA-MEC with WPT system under Nakagami-m fading channels for IoT networks, with the interference of an passive eavesdropper. Additionally, the study enhances the communication interchanges between UAV and edge devices (EDs) by employing the probabilistic models of LoS and non-LoS (NLoS) propagation. The primary contributions of our paper are as follows:

- We investigate the secrecy offloading efficiency for an UAV-assisted NOMA-integrated MEC processor incorporating WPT within an IoT network. Hence, we introduce a system protocol that ensures an efficient wireless charging and offloading operation.
- The secrecy successful computation probability (SSCP) closed-formed formulation of the whole system in regards of imperfect channel state information (iCSI) and imperfect successive interference cancellation (iSIC) is derived.
- Theoretical findings are conducted with a variety of parameters including UAV's transmission power, the num-

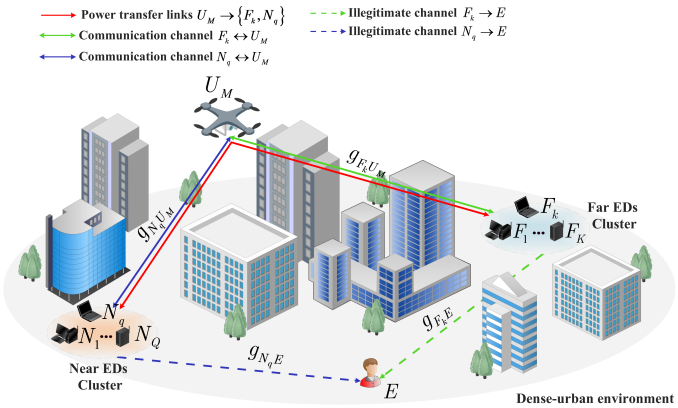

Fig. 1: System model of the UAV-assisted uplink NOMA-MEC with WPT in IoT networks.

ber of EDs, network parameters, energy harvesting (EH) ratio, and the UAV's positions and altitudes, thereby validating the precision of our analysis.

The paper's remaining sections are structured thusly as. Section II provides insights of the system model's characteristics and its protocol. Thereafter, Section III delves into the derivation of the SSCP formulation. Section IV discusses the theoretical findings. Eventually, Section V presents the conclusions of this study.

II. System Model and Protocol

A. System and Channel Model

Fig. 1 illustrates a system model of a dense-urban scenario in the IoT networks comprising of an UAV-assisted NOMA-integrated MEC processor, denoted by U_M, a remote cluster of EDs (F_k) with K devices, and a nearby EDs cluster (N_q) with Q devices, where $k \in \{1, ..., K\}$ and $q \in \{1, ..., Q\}$. Particularly, U_M initiates the system operations by broadcasting the wireless power via radio frequency signals to the two edge clusters. These signals are then harvested by those power-constrained EDs. Following the EH phase, a selection process is employed to identify the ED with the highest computational efficiency from each cluster, which is utilized to perform secure data offloading tasks to the U_M by uplink NOMA, with the interference of an passive eavesdropper (E). All devices are assumed to be equipped with a single antenna and operate in a half-duplex mode.

Furthermore, it is posited that each ED carries out identical workloads with length l (bits), and these tasks are independently separated into distinctive groups. Thus, the offloading capacities of the EDs are expressed as [10] $\mathcal{C}_{\vartheta}^{off} = \sigma_{\vartheta} l$, where σ_{ϑ} represents the offloading ratio, with $(0 < \sigma_{\vartheta} < 1)$, and $\vartheta \in (F_k, N_q)$.

To model spatial relationships of the system components, we exploit a 3D Cartesian coordinate system, in which the UAV's coordinate is $U_M\,(x_U, y_U, h_U)$, while the ground nodes are denoted as $F_k\,(x_k, y_k, 0)$, $N_q\,(x_q, y_q, 0)$, and $E\,(x_E, y_E, 0)$. Assuming that the large-scale fading channel between UAV and EDs is characterized by the probabilistic model of LoS and NLoS propagation. Thus, the mean path-loss is expressed as follows [7]:

$$\overline{\mathbb{L}}_{ab} = \left[\mathbb{K}^{NLoS} + \frac{\mathbb{K}^{LoS} - \mathbb{K}^{NLoS}}{1 + \tau_1 e^{\left(-\frac{180}{\pi}\tau_2 \varphi_{ab} + \tau_2 \tau_1\right)}} \right] \mathbb{D}_{ab}^{\theta}, \quad (1)$$

where $ab \in \{F_k U_M, N_q U_M, F_k E, N_q E\}$, $\mathbb{K}^{LoS} = \mu^{LoS}\left(\frac{c}{4\pi f_c}\right)^{-1}$, $\mathbb{K}^{NLoS} = \mu^{NLoS}\left(\frac{c}{4\pi f_c}\right)^{-1}$, c and f_c are the speed of light and the carrier frequency, respectively; μ^{LoS} and μ^{NLoS} are the excessive path-losses of LoS and NLoS connections; τ_1 and τ_2 are the parameters that vary depending on the surrounding environments; $\varphi_{ab} = \arcsin(\frac{h_U}{\mathbb{D}_{ab}})$ is the elevation angle; $\mathbb{D}_{ab} = \sqrt{(x_b - x_a)^2 + (y_b - y_a)^2 + (h_b - h_a)^2}$ is the distance of ab; θ is the path-loss exponent.

It is assumed that the channel coefficients, denoted as g_{ab}, are independent, and conform the Nakagami-m fading model. Nevertheless, due to the feedback latencies, the system model is inevitably affected by the iCSI [10]. Thus, the channel coefficient is calculated as: $g_{ab} = \tilde{g}_{ab} + \lambda_{ab}$, where $\tilde{g}_{ab}$ is the estimated channel coefficient, λ_{ab} is the channel quality parameter, $\lambda_{ab} \sim \mathcal{CN}(0, \Omega_{ab})$. Within this paper, the channel quality variance Ω_{ab} is considered to be constant [14].

Given that the all channel coefficient are affected by the Nakagami-m fading model, the probability density function (PDF) and cumulative distribution function (CDF) of the channel coefficients $|\tilde{g}_{\vartheta^* E}|^2$ detected at E is expressed as [8]:

$$f_{|\tilde{g}_{\vartheta^* E}|^2}(u) = \frac{u^{m-1}}{(m-1)!}\left(\frac{m}{\xi_{\vartheta^* E}}\right)^m e^{-\frac{mu}{\xi_{\vartheta^* E}}}, \quad (2)$$

$$F_{|\tilde{g}_{\vartheta^* E}|^2}(u) = 1 - e^{-\frac{mu}{\xi_{\vartheta^* E}}} \sum_{s=0}^{m-1} \frac{1}{s!}\left(\frac{mu}{\xi_{\vartheta^* E}}\right)^s. \quad (3)$$

Accordingly, by calculating the maximal signal-to-noise ratios (SNRs) among U_M, F_k, and N_q connections, the channel gains for the two best EDs in the respective clusters are represented as: $|\tilde{g}_{\vartheta^* U}|^2 = \max\left\{|\tilde{g}_{\vartheta U_M}|^2\right\}$, where $\vartheta^* \in (F^*, N^*)$. Thus, the PDF and CDF of the estimated channel coefficients $|\tilde{g}_{\vartheta^* U}|^2$ detected at U_M can be expressed as [13]:

$$f_{|\tilde{g}_{\vartheta^* U}|^2}(u) = \ddot{\mathcal{Z}} \sum_{p} (\mathcal{Z} - 1)\, u^{m-1+\bar{p}} e^{-\frac{um}{\xi_{\vartheta^* U}}(p+1)}, \quad (4)$$

$$F_{|\tilde{g}_{\vartheta^* U}|^2}(u) = \sum_{p} (\mathcal{Z})\, u^{\bar{p}} e^{-\frac{pum}{\xi_{\vartheta^* U}}}, \quad (5)$$

where $\mathcal{Z} \in \{K, Q\}$, $p \in \{h, t\}$, $\sum_{p}(\mathcal{Z} - 1) = \sum_{p=0}^{\mathcal{Z}-1} \Xi_p (-1)^p \Phi_{1,p} \Phi_{2,p}$, $\Xi_p = \sum_{p_1=0}^{p} \sum_{p_2=0}^{p-p_1} \cdots \sum_{p_{m-1}=0}^{p-\ldots-p_{m-2}}$, $\Phi_{1,p} = \binom{\mathcal{Z}-1}{p}\binom{p}{p_1}\binom{p-p_1}{p_2}\ldots\binom{p-\ldots-p_{m-2}}{p_{m-1}}$, $\Phi_{2,p} = \prod_{s=0}^{m-2}\left[\frac{1}{s!}\left(\frac{m}{\xi_{\vartheta^* U}}\right)^s\right]^{p_{s+1}} \left[\frac{1}{(m-1)!}\left(\frac{m}{\xi_{\vartheta^* U}}\right)^{m-1}\right]^{p-\ldots-p_{m-1}}$, $\ddot{\mathcal{Z}} = \frac{\mathcal{Z}}{(m-1)!}\left(\frac{m}{\xi_{\vartheta^* U}}\right)^m$, $\bar{p} = (m-1)(p-p_1) - (m-2)p_2 - \ldots - p_{m-1}$, $m \in (2, 3, 4, ...)$.

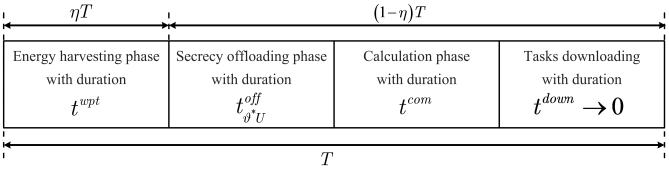

Fig. 2: The protocol flowchart for the UAV-assisted NOMA-MEC with WPT system.

B. System Protocol

This subsection introduces an quad-phased protocol for the proposed system. Specifically, the protocol flowchart in Fig 2 is described as follows:

- In the energy harvesting phase, denoted as t^{wpt}: U_M initially sends the radio frequency signals to the ED clusters to harvest energy. Subsequently, the two best EDs from their respective clusters are chosen based on the highest SNRs. Therefore, the energy conveyed to the EDs is formulated as: $E_{\vartheta^* U} = \frac{\beta P_U t^{wpt} |g_{\vartheta^* U}|^2}{\overline{\mathbb{L}}_{\vartheta^* U}}$, where β is the energy conversion coefficient, $(0 < \beta < 1)$; P_U denotes the U_M transmitted power; $t^{wpt} = \eta T$, η is the EH ratio, $(0 < \eta < 1)$; and T is the protocol execution time.
- In the secrecy offloading phase, denoted as $t^{off}_{\vartheta^*}$: the selected EDs concurrently offload their tasks via uplink NOMA resulting in the composite signal obtained at U_M as: $y^{MEC}_U = \sqrt{\frac{\rho_{F^* U} P_{F^* U}}{\overline{\mathbb{L}}_{F^* U}}} \left(\tilde{g}_{F^* U} + \lambda_{F^* U}\right) x_{F^* U} + \sqrt{\frac{\rho_{N^* U} P_{N^* U}}{\overline{\mathbb{L}}_{N^* U}}} \left(\tilde{g}_{N^* U} + \lambda_{N^* U}\right) x_{N^* U} + n_U$, where ρ is the power allocation ratio $(\rho_{F^* U} + \rho_{N^* U} = 1, \ \rho_{F^* U} > \rho_{N^* U})$; $P_{\vartheta^* U} = \frac{E_{\vartheta^* U}}{(1-\eta)T - t^{com}}$ is the power transmit of EDs to U_M; $x_{\vartheta^* U}$ is the transmitted signal of the optimal EDs; n_U is subject to the additive white Gaussian noise (AWGN) distribution, with $n_U \sim \mathcal{CN}(0, \mathcal{N}_U)$. In the decoding processes, by following the NOMA principles, U_M initially tackles the x_{F^*} signal by treating x_{N^*} as interference. Thereafter, U_M implements SIC to extract the preceding decoded signal. Hence, the expressions for the signal-to-interference-plus-noise ratios (SINRs) at U is expressed as [13]:

$$\gamma^U_{F^*} = \frac{z_1 a^2}{z_2 b^2 + z_3}, \gamma^U_{N^*} = \frac{z_2 b^2}{\nu_1 z_1 a^2 + z_4}, \tag{6}$$

where $z_1 = \frac{\gamma_{F^* U}}{\overline{\mathcal{L}}_{F^* U}}$, $z_2 = \frac{\gamma_{N^* U}}{\overline{\mathcal{L}}_{N^* U}}$, $z_3 = z_1 \Omega^2_{F^* U} + z_2 \Omega^2_{N^* U} + 1$, $z_4 = \nu_1 z_1 \Omega^2_{F^* U} + z_2 \Omega^2_{N^* U} + 1$, $\gamma_{F^* U} = \frac{\rho_{F^* U} \beta \gamma_U \eta T}{\overline{\mathbb{L}}_{F^* U}[(1-\eta)T - t^{com}]}$, $\gamma_{N^* U} = \frac{\rho_{N^* U} \beta \gamma_U \eta T}{\overline{\mathbb{L}}_{N^* U}[(1-\eta)T - t^{com}]}$, $\gamma_U = \frac{P_U}{\mathcal{N}_U}$, $a = |\tilde{g}_{F^* U}|^2$, $b = |\tilde{g}_{N^* U}|^2$, ν_1 denotes the residual interference caused by the iSIC, with $(0 \le \nu_1 \le 1)$, and $\nu_1 = 0$ represents the ideal system decoding, namely perfect SIC (pSIC). Similarly, the expressions of composite signals at E is expressed as: $y_E = \sqrt{\frac{\rho_{F^* E} P_E}{\mathbb{L}_{F^* E}}} \left(\tilde{g}_{F^* E} + \lambda_{F^* E}\right) x_{F^* E} + \sqrt{\frac{\rho_{N^* E} P_E}{\mathbb{L}_{N^* E}}} \left(\tilde{g}_{N^* E} + \lambda_{N^* E}\right) x_{N^* E} + n_E$, where $\rho_{F^* E} + \rho_{N^* E} = 1$, $(\rho_{F^* E} > \rho_{N^* E})$, $n_E \sim \mathcal{CN}(0, \mathcal{N}_E)$. Supposing E also conforms SIC principal, the expressions of the SINRs at E is given as [8]:

$$\gamma^E_{F^*} = \frac{z_5 x}{z_6 y + z_7}, \gamma^E_{N^*} = \frac{z_6 y}{z_8}, \tag{7}$$

where $z_5 = \frac{\rho_{F^* E} \gamma_E}{\mathbb{L}_{F^* E}}$, $z_6 = \frac{\rho_{N^* E} \gamma_E}{\mathbb{L}_{N^* E}}$, $z_7 = z_5 \Omega_{F^* E} + z_6 \Omega_{N^* E} + 1$, $z_8 = z_6 \Omega_{N^* E} + 1$, $\gamma_E = \frac{P_E}{\mathcal{N}_E}$, $x = |\tilde{g}_{F^* E}|^2$, $y = |\tilde{g}_{N^* E}|^2$.
- In the third phase, denoted as t^{com}: The offloaded tasks are calculated at U_M. The duration necessary for the accomplishment of these computational processes with a number of task bits is expressed as: $t^{com} = \frac{(\mathcal{C}^{off}_{q^*} + \mathcal{C}^{off}_{j^*})\varpi}{f_{MEC}}$, where ϖ is the number of CPU cycles requires to compute a single task bit and f_{MEC} is the MEC's operating frequency at U_M.
- In the fourth phase, denoted as t^{down}: Eventually, U_M transfers the outcomes to the edge clusters through their corresponding optimal ED. Notably, due to the minimal energy depletion and brief latency associated with the data retrieval, the t^{down} phase can be negligible [15].

III. Secrecy Offloading Efficacy Analysis

A. Preliminaries

In the proposed system, the channel capacity of UAV U_M and that of eavesdropper E to detect the best remote/nearby EDs are given as follows, respectively:

$$C^U_{\vartheta^*} = [(1-\eta)T - t^{com}] W \log_2\left(1 + \gamma^U_{\vartheta^*}\right), \tag{8}$$
$$C^E_{\vartheta^*} = [(1-\eta)T - t^{com}] W \log_2\left(1 + \gamma^E_{\vartheta^*}\right), , \tag{9}$$

where W is the system bandwidth. Thus, the secrecy capacity of EDs to U_M, with the interference of an passive eavesdropper is characterized as follows:

$$\begin{aligned} C^S_{\vartheta^*} &= \left[C^U_{\vartheta^*} - C^E_{\vartheta^*}\right]^+ \\ &= \begin{cases} [(1-\eta)T - t^{com}] W \log_2\left(\frac{1+\gamma^U_{\vartheta^*}}{1+\gamma^E_{\vartheta^*}}\right), & \gamma^U_{\vartheta^*} > \gamma^E_{\vartheta^*} \\ 0, & \gamma^U_{\vartheta^*} \le \gamma^E_{\vartheta^*} \end{cases}, \end{aligned} \tag{10}$$

B. Secrecy successful computation probability (SSCP)

To assess the system's secrecy offloading efficacy, this subsection delves into the derivation of the SSCP formulation of the whole system, denoted by $\mathcal{S}_{s^*}$. The SSCP is determined as the likelihood that the duration of the offloaded tasks $t^{off}_{\vartheta^*}$ accomplishes within the prescribed latency threshold T_{th}, while the secrecy capacity $C^S_{\vartheta^*}$ functions above a predetermined rate R_{ϑ^*}. Thus, the SSCP of the whole system is expressed as:

$$\mathcal{S}_{s^*} = \Pr\left\{t^{off}_{F^*} \le T_{th}, t^{off}_{N^*} \le T_{th}, C^S_{F^*} \ge R_{F^*}, C^S_{N^*} \ge R_{N^*}\right\}, \tag{11}$$

where $t^{off}_{\vartheta^*} = \frac{\mathcal{C}^{off}_{\vartheta^*}}{C_{\vartheta^*}}$, and $R_{\vartheta^*} = \frac{\mathcal{C}^{off}_{\vartheta^*}}{T_{th}}$. We assume that $T_{th} = (1-\eta)T - t^{com}$. Hence, the closed-formed formulation of SSCP is expressed as in *Lemma 1* and *Lemma 2*.

Lemma 1: The closed-form formulation for the SSCP of the whole system under Nakagami-m fading channel in the case of iSIC is derived as:

$$\mathcal{S}_{s^*,1} = \psi_{1,c} \sum_{h} (Q-1) \sum_{t} (K-1)\, \Psi_1^{(\wp_o)} \Psi_2^{(\omega_n)} \times \left[\delta_1 - \delta_2^{(\Delta_4)} - \delta_3^{(\Theta_1)} \left(\delta_4^{(\Theta_1)} - \delta_5^{(\Delta_4,\Theta_3)}\right)\right],$$

where $\psi_{1,c} = \frac{\pi^2 \ddot{K}\ddot{Q}}{4NO(m-1)!}\left(\frac{m}{\xi_{N^*E}}\right)^m$, $\Psi_1^{(\wp_o)} = \sum_{o=1}^{O} \sqrt{1-\varphi_o^2} \frac{\wp_o^{m-1+\bar{h}} \omega_o^{\frac{\wp_o^2 m(h+1)}{\xi_{N^*U}}-1} \left(\Delta_3^{(\wp_o)} - \Delta_1^{(\wp_o)}\right)}{\ln^2(\omega_o)}$, $\Psi_2^{(\omega_n)} = \sum_{n=1}^{N} \sqrt{1-\varphi_n^2} \omega_n^{m-1+\bar{t}} e^{-\frac{m(t+1)}{\xi_{F^*U}}\omega_n}$, $\delta_1 = \frac{(m-1)!}{(m/\xi_{N^*E})^m}$, $\delta_2^{(\Delta_4)} = e^{\frac{-m}{\xi_{N^*E}}\Delta_4^{(\omega_n,\wp_o)}} \sum_{k_1=0}^{m-1} \frac{(m-1)!}{k_1!} \frac{\left(\Delta_4^{(\omega_n,\wp_o)}\right)^{k_1}}{(m/\xi_{N^*E})^{m-k_1}}$, $\delta_3^{(\Theta_1)} = e^{\frac{-m}{\xi_{F^*E}}\Theta_1^{(\omega_n,\wp_o)}} \sum_{s=0}^{m-1} \frac{1}{s!}\left(\frac{m}{\xi_{F^*E}}\right)^s \sum_{k_2=0}^{s} \binom{s}{k_2} \left(\frac{z_6}{z_7}\right)^{k_2} \times \left(\Theta_1^{(\omega_n,\wp_o)}\right)^s$, $\delta_4^{(\Theta_1)} = \frac{(m-1+k_2)!}{\left(\Theta_3^{(\omega_n,\wp_o)}\right)^{m+k_2}}$, $\delta_5^{(\Delta_4,\Theta_3)} = e^{-\Delta_4^{(\omega_n,\wp_o)}\Theta_3^{(\omega_n,\wp_o)}} \sum_{k=0}^{m-1+k_2} \frac{(m-1+k_2)!}{k!} \frac{\left(\Delta_4^{(\omega_n,\wp_o)}\right)^k}{\left(\Theta_3^{(\omega_n,\wp_o)}\right)^{m+k_2-k}}$. The mentioned Δ_1, Δ_3, Δ_4, Θ_1, Θ_3 are characterized as:

$$\Delta_1^{(\wp_o)} = \sqrt{\frac{\zeta_{F^*}\left(z_2\wp_o^2 + z_3\right)}{z_1}}, \tag{12}$$

$$\Delta_3^{(\wp_o)} = \sqrt{\frac{z_2\wp_o^2 - z_4\zeta_{N^*}}{\nu_1 z_1 \zeta_{N^*}}}, \tag{13}$$

$$\Delta_4^{(\omega_n,\wp_o)} = \left(1 + \frac{z_2\wp_o^2}{\nu_1 z_1 \omega_n^2 + z_4} - \partial_{N^*}\right)\frac{z_8}{z_6\partial_{N^*}}, \tag{14}$$

$$\Theta_1^{(\omega_n,\wp_o)} = \left(1 + \frac{z_1\omega_n^2}{z_2\wp_o^2 + z_3} - \partial_{F^*}\right)\frac{z_7}{z_5\partial_{F^*}}, \tag{15}$$

$$\Theta_3^{(\omega_n,\wp_o)} = \left(\frac{m}{\xi_{N^*E}} + \frac{m z_6 \Theta_1^{(\omega_n,\wp_o)}}{\xi_{F^*E} z_7}\right), \tag{16}$$

where $\wp_o = -\frac{1}{\ln(\omega_o)}$, $\omega_o = \frac{\varphi_o+1}{2}$, $\varphi_o = \cos\left(\frac{\pi(2o-1)}{2O}\right)$, $\omega_n = \frac{(\varphi_n+1)\left(\Delta_3^{(\wp_o)} - \Delta_1^{(\wp_o)}\right)}{2} + \Delta_1^{(\wp_o)}$, $\varphi_n = \cos\left(\frac{\pi(2n-1)}{2N}\right)$, $\zeta_{\vartheta^*} = 2^{\frac{c_{\vartheta^*}^{off}}{W(T_{th})^2}} - 1$, $\partial_{\vartheta^*} = 2^{\frac{R_{\vartheta^*}}{WT_{th}}}$, N and O are the complexity versus accuracy trade-off coefficient [17].

Proof 1: See Appendix A.

Lemma 2: The closed-form formulation for the SSCP of the whole system under Nakagami-m fading channel in the case of pSIC is express as::

$$\mathcal{S}_{s^*,2} = \psi_{2,c} \sum_{h} (Q-1) \sum_{t} (K-1)\, \Psi_3^{(\wp_o)} \left[\Psi_4^{(\Delta_1)} \times \left(\delta_1 - \delta_6^{(\Delta_5)}\right) - \Psi_5^{(\Delta_1)} \delta_7^{(\Theta_1)} \left(\delta_8^{(\Theta_3)} - \delta_9^{(\Delta_5,\Theta_3)}\right)\right],$$

where $\psi_{2,c} = \frac{\pi e^{-\Delta_2} \ddot{K}\ddot{Q}}{2O(m-1)!}\left(\frac{m}{\xi_{N^*E}}\right)^m$, $\Psi_3^{(\wp_o)} = \sum_{o=1}^{O} \sqrt{1-\varphi_o^2} \wp_o^{m-1+\bar{h}} \omega_o^{\frac{m(h+1)}{\xi_{N^*U}}-1}$, $\Psi_4^{(\Delta_1)} = e^{-\frac{m(t+1)}{\xi_{F^*U}}\Delta_1^{(\wp_o)}} \sum_{k_3=0}^{m-1+\bar{t}} \frac{(m-1+\bar{t})!}{k_3!} \frac{\left(\Delta_1^{(\wp_o)}\right)^{k_3}}{(m(t+1)/\xi_{F^*U})^{m+\bar{t}-k_3}}$, $\delta_6^{(\Delta_5)} = e^{\frac{-m}{\xi_{N^*E}}\Delta_5^{(\wp_o)}} \sum_{k_1=0}^{m-1} \frac{(m-1)!}{k_1!} \frac{\left(\Delta_5^{(\wp_o)}\right)^{k_1}}{(m/\xi_{N^*E})^{m-k_1}}$, $\Psi_5^{(\Delta_1)} = \frac{\pi e^{-\Delta_1^{(\wp_o)}}}{2N} \sum_{n=1}^{N} \sqrt{1-\varphi_n^2} \wp_n^{m-1+\bar{t}} \omega_n^{\frac{m(t+1)}{\xi_{F^*U}}-1}$, $\delta_7^{(\Theta_1)} = e^{\frac{-m}{\xi_{F^*E}}\Theta_1^{(\wp_n,\wp_o)}} \sum_{s=0}^{m-1} \frac{1}{s!}\left(\frac{m}{\xi_{F^*E}}\right)^s \sum_{k_2=0}^{s} \binom{s}{k_2} \left(\frac{z_6}{z_7}\right)^{k_2} \left(\Theta_1^{(\wp_n,\wp_o)}\right)^s$, $\delta_8^{(\Theta_3)} = \frac{(m-1+k_2)!}{\left(\Theta_3^{(\wp_n,\wp_o)}\right)^{m+k_2}}$, $\delta_9^{(\Delta_5,\Theta_3)} = e^{-\Delta_5^{(\wp_o)}\Theta_3^{(\wp_n,\wp_o)}} \times \sum_{k=0}^{m-1+k_2} \frac{(m-1+k_2)!}{k!} \frac{\left(\Delta_5^{(\wp_o)}\right)^k}{\left(\Theta_3^{(\wp_n,\wp_o)}\right)^{m+k_2-k}}$, $\Delta_2 = \sqrt{\frac{z_4\zeta_{N^*}}{z_2}}$, $\Delta_5^{(\wp_o)} = \left(1 + \frac{z_2\wp_o^2}{z_4} - \partial_{N^*}\right)\frac{z_8}{z_6\partial_{N^*}}$. Noted in this pSIC scenario, we assume that $\wp_o = -\ln(\omega_o)$, $\omega_o = \frac{(\varphi_o+1)e^{-\Delta_2}}{2}$, $\wp_n = -\ln(\omega_n)$, $\omega_n = \frac{(\varphi_n+1)e^{-\Delta_1^{(\wp_o)}}}{2}$.

Proof 2: See Appendix B.

IV. Numerical Results

This section presents the theoretical findings that verifies the offloading performance of the considered system. The parameter values across all the simulations is specified as follows: $(x_U, y_U) = (0,0)$, $h_U \in (50, 300)$ (m), $(x_F, y_F) = (-100, -100)$ (m), $(x_N, y_N) = (10, 10)$ (m), $(x_E, y_E) = (80, 80)$ (m), $\theta = 2$, $\mu^{LoS} = 1.6$, $\mu^{NLoS} = 23$, $\tau_1 = 0.1139$, $\tau_2 = 12.0870$, $c = 3.10^8$, $f_c = 10^5$ (Hz), $W = 10^2$ (MHz), $\gamma_U \in [0, 40]$ (dB), $\eta \in [0, 1]$, $\beta = 0.9$, $T = 1$ (s), $\sigma_{F^*} = \sigma_{N^*} = 0.5$, $l = 10^2$ (bits), $\rho = 0.8$, $f_{MEC} = 10^8$ (Hz), $\varpi = 10^2$, $m = 2$, $N = O = 10^3$.

As shown in Fig. 3-7, the concurrence of the simulation (Sim.) and the theoretical study (Ana.) validates our system analysis. Fig. 3 depicts the effect of UAV's transmission power (γ_U) on SSCP of the whole system, with a multitude of EDs (K and Q). The figure indicates that a concurrent rise in the device quantity enhances SSCP. This can be referred to an enlarged option of EDs, offering the UAV greater selection flexibility on secure data offloading. Additionally, an increased transmission source γ_U boosts the SSCP, allowing EDs to posses plenty of power for an effective offloading operation.

Fig. 4 demonstrates the effect of CSI and SIC parameters on the SSCP of the whole system. The observation shows that the maximal system's secrecy offloading efficiency can be obtained under the state of pCSI-pSIC. Nonetheless, the broadcast nature of channel conditions, associated with the inherent limitations in hardware, inevitably results in iCSI-iSIC scenarios, thereby degrading the system performance.

Fig. 5 illustrates the effect of UAV's altitudes on SSCP of the whole system. The result displays ideal points of UAV's altitude h_U^* that achieve the desirable SSCP values. This is attributed to the interchange between LoS and NLoS signal propagation of UAV-EDs reception. Elevating UAV's altitude initially favors strong LoS conditions, while an excessive altitude introduces greater path loss, consequently hindering the system secrecy efficacy.

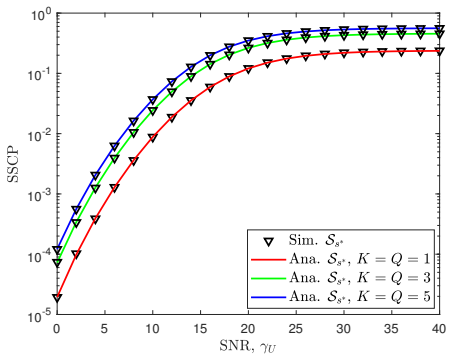

Fig. 3: Effect of UAV's average transmit SNR, γ_U on SSCP of the whole system with a variety of EDs, with $\gamma_E = 10$ (dB), $h_U = 50$ (m), $\eta = 0.7$, $\Omega = 3$, and $\nu_1 = 0.4$.

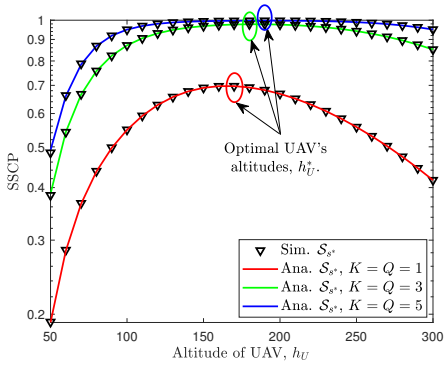

Fig. 5: Effect of UAV's altitude, h_U on SSCP of the whole system with a variety of EDs, with $\gamma_U = 30$ (dB), $\gamma_E = 10$ (dB), $\eta = 0.4$, $\Omega = 3$, and $\nu_1 = 0.4$.

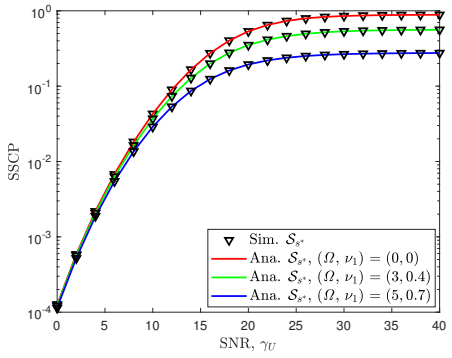

Fig. 4: Effect of CSI parameters Ω and SIC parameters ν_1 on SSCP of the whole system, with $K = Q = 5$, $\gamma_E = 10$ (dB), $h_U = 50$ (m), and $\eta = 0.7$.

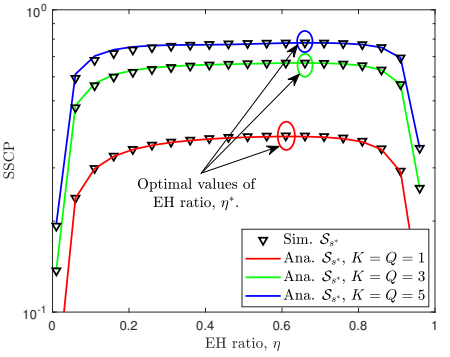

Fig. 6: Effect of EH ratio, η on SSCP of the whole system with a variety of EDs, with $\gamma_U = 38$ (dB), $\gamma_E = 10$ (dB), $h_U = 60$ (m), $\Omega = 3$, and $\nu_1 = 0.4$.

Fig. 6 depicts the effect of EH ratio (η) on SSCP of the whole system. It identifies the optimal values of EH ratio η^* that maximize SSCP. As the increase in η allows EDs to allocate more time for energy acquisition, thus diminishing the duration available for secrecy offloading operation. Alternatively, the decrease in η results in the reduction of EH time, restricting energy capacity of EDs to offload tasks.

To capitalize on the LoS utility, the deployments of UAV's positions is crucial for enhancing transmission link strength. Fig. 7 depicts the effect of (x_U, y_U) on SSCP of the whole system. The finding displays an optimal position (x_U^*, y_U^*) that optimizes SSCP. This finding is consistent with the intuition of the UAV's strategic placements for optimal communication.

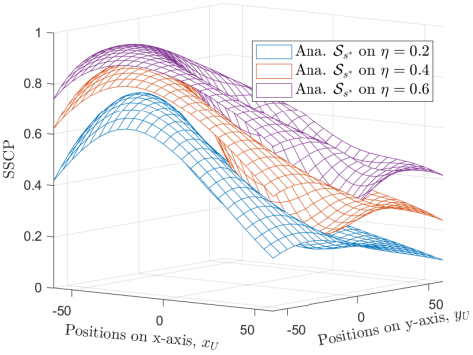

Fig. 7: Effect of UAV's position, (x_U, y_U) on SSCP of the whole system with $K = Q = 1$, $\gamma_U = 34$ (dB), $\gamma_E = 10$ (dB), $h_U = 60$ (m), $\eta = 0.4$, $\Omega = 3$, and $\nu = 0.4$.

V. Conclusion

In this paper, we studied an UAV-assisted NOMA-integrated MEC with WPT under Nakagami-m fading channel in IoT networks. We introduced a quad-phased system protocol that ensures an efficient wireless charging and offloading operation. The SSCP closed-form formulations were expressed for the system's secrecy offloading efficacy assessments. Eventually, the theoretical findings were conducted with a variety of parameters that verifies the efficiency of the considered system.

Appendix A.

By substituting the (6), (7), (8), (10) into the defined formula of (11), $\mathcal{S}_{s^*,1}$ in the scenario of $\nu > 0$ can be expressed as:

$$\mathcal{S}_{s^*,1} = \int_0^{\infty} \int_{\Delta_1^{(b)}}^{\Delta_3^{(b)}} \int_0^{\Delta_4^{(a,b)}} F_x \left[\left(1 + \frac{z_1 a^2}{z_2 b^2 + z_3} - \partial_{F^*} \right) \frac{z_6 y + z_7}{z_5 \partial_{F^*}} \right] \times f_y(y) f_a(a) f_b(b) \, dy da db, \quad (17)$$

where $\Delta_1^{(b)} = \sqrt{\frac{\zeta_{F^*}(z_2 b^2+z_3)}{z_1}}$, $\Delta_3^{(b)} = \sqrt{\frac{z_2 b^2 - z_4 \zeta_{N^*}}{\psi_1 z_1 \zeta_{N^*}}}$, $\Delta_4^{(a,b)} = \left(1+\frac{z_2 b^2}{\nu_1 z_1 a^2+z_4} - \partial_{N^*}\right)\frac{z_8}{z_6 \partial_{N^*}}$. Thereby integrating (2) and (3) into (17), the first integral of $\mathcal{S}_{s^*,1}$ is derived as:

$$I_1 = \frac{1}{(m-1)!}\left(\frac{m}{\xi_{N^*E}}\right)^m \left(\int_0^{\Delta_4^{(a,b)}} y^{m-1} e^{-\frac{my}{\xi_{N^*E}}} dy \right.$$
$$- \int_0^{\Delta_4^{(a,b)}} y^{m-1} e^{\frac{-my}{\xi_{N^*E}}} e^{\frac{-m}{\xi_{F^*E}}\left(1+\frac{z_1 a^2}{z_2 b^2+z_3}-\partial_{F^*}\right)\frac{z_6 y+z_7}{z_5 \partial_{F^*}}} \sum_{s=0}^{m-1} \frac{1}{s!}$$
$$\left. \times \left(\frac{m}{\xi_{F^*E}}\right)^s \left[\left(1+\frac{z_1 a^2}{z_2 b^2+z_3} - \partial_{F^*}\right)\frac{z_6 y+z_7}{z_5 \partial_{F^*}}\right]^s dy \right). \tag{18}$$

The first integral of (18) can be solved by adopting the equation 3.351.1.[8] in [16]. Thereafter, the equation 1.111 of [16] is exploited in the second integral of (18) for further analysis. Similarly applying the method in the I_1 first integral for the second integral, the completed expression of I_1 is achieved as:

$$I_1 = \frac{1}{(m-1)!}\left(\frac{m}{\xi_{N^*E}}\right)^m \left[\frac{(m-1)!}{\left(\frac{m}{\xi_{N^*E}}\right)^m} - e^{\frac{-m}{\xi_{N^*E}}\Delta_4^{(a,b)}} \sum_{k_1=0}^{m-1} \right.$$
$$\frac{(m-1)!}{k_1!} \frac{\left(\Delta_4^{(a,b)}\right)^{k_1}}{\left(\frac{m}{\xi_{N^*E}}\right)^{m-k_1}} - e^{\frac{-m}{\xi_{F^*E}}\Theta_1^{(a,b)}} \sum_{s=0}^{m-1} \frac{1}{s!}\left(\frac{m}{\xi_{F^*E}}\right)^s$$
$$\times \sum_{k_2=0}^{s} \binom{s}{k_2} \left(\frac{z_6}{z_7}\right)^{k_2} \left(\Theta_1^{(a,b)}\right)^s \left(\frac{(m-1+k_2)!}{\left(\Theta_3^{(a,b)}\right)^{m+k_2}} \right.$$
$$\left. \left. - e^{-\Delta_4^{(a,b)}\Theta_3^{(a,b)}} \sum_{k=0}^{m-1+k_2} \frac{(m-1+k_2)!}{k!} \frac{\left(\Delta_4^{(a,b)}\right)^k}{\left(\Theta_3^{(a,b)}\right)^{m+k_2-k}} \right) \right]. \tag{19}$$

Combining with (4), (5), and (19), the second and final integral of $\mathcal{S}_{s^*,1}$ can be sequentially resolved with the aid of the Gaussian-Chebyshev Quadrature in [17]. Thus, the closed-formed formulation of SSCP for the whole system in the case of iSIC is derived as in *Lemma 1*.

Appendix B.

Similarly substituting as (17), $\mathcal{S}_{s^*,2}$ in the scenario of $\nu = 0$ can be given as:

$$\mathcal{S}_{s^*,1} = \int_{\Delta_2}^{\infty} \int_{\Delta_1^{(b)}}^{\infty} \int_0^{\Delta_5^{(b)}} F_x\left(\left(1+\frac{z_1 a^2}{z_2 b^2+z_3} - \partial_{F^*}\right)\frac{z_6 y+z_7}{z_5 \partial_{F^*}}\right)$$
$$\times f_y(y) f_a(a) f_b(b) \, dy da db, \tag{20}$$

where $\Delta_5^{(b)} = \left(1+\frac{z_2 b^2}{z_4} - \partial_{N^*}\right)\frac{z_8}{z_6 \partial_{N^*}}$. The completed expression of the first integral in this case, denoted as I_3, is identically obtained as in (19). Hence, the expression of the second integral of $\mathcal{S}_{s^*,2}$ is obtained as:

$$I_4 = \int_{\Delta_1^{(b)}}^{\infty} f_a(a) I_3 da. \tag{21}$$

By substituting (4) into (21) and employing the distributive property, the I_4 integrals are achieved through the application of the equation 3.351.2.[11] in [16] and the Gaussian-Chebyshev Quadrature method in [17]. Eventually, the final integral is addressed by exploiting (4) along with the Quadrature method. Thus, the closed-formed formulation of SSCP for the whole system in the case of pSIC is derived as in *Lemma 2*.

References

[1] Z. Zhi, "Research and Design of Industrial IoT Device Management System Based on 5G Communication and Big Data Technology," 2nd ISPCEM, 2022.

[2] J. Cook, Sabih ur Rehman, and M. Arif Khan, "Security and Privacy for Low Power IoT Devices on 5G and Beyond Networks: Challenges and Future Directions," IEEE Access, vol.11, 2023.

[3] A.-N. Nguyen, D.-B. Ha, V. N. Vo, V.-T. Truong, D.-T. Do, and C. So-In, "Performance Analysis and Optimization for IoT Mobile Edge Computing Networks With RF Energy Harvesting and UAV Relaying," IEEE Access, vol. 10, pp. 21526-21540, 2021.

[4] S. Ahmed, Z. Subah, and M. Z. Ali, "Cryptographic Data Security for IoT Healthcare in 5G and Beyond Networks," IEEE Sensors, 2022.

[5] P. Shrivastava, Meeradevi, and M. R Mundada, "Survey on Congestion Control Approaches in 4G/5G Cellular Networks," 4th I4C, 2022.

[6] N. Wang, P. Wang, A. A.-Fanid, L. Jiao, and K. Zeng, "Physical Layer Security of 5G Wireless Networks for IoT: Challenges and Opportunities," IEEE Int. of Things J., vol.6, no. 5, pp. 8169-8181, 2019.

[7] R. Zhang, X. Pang, J. Tang, Y. Chen; N. Zhao, and X. Wang, "Joint Location and Transmit Power Optimization for NOMA-UAV Networks via Updating Decoding Order," IEEE Wireless Communications Letters, vol. 10, no. 1, pp. 136-140, 2021.

[8] A.-N. Nguyen, T.-S. Ngo, N.-A. Bui, P.-C. Le, and G.-H. Nguyen, "UAV-aided uplink NOMA based on MEC in IoT networks: Secrecy offloading and Optimization," SaSeIoT, pp. 131-146, 2024.

[9] A.-N. Nguyen, D.-B. Ha, V.-T. Truong, C. So-In, P. Aimtongkham, C. Sakunrasrisuay, and C. Punriboon, "On Secrecy Analysis of UAV-Enabled Relaying NOMA Systems with RF Energy Harvesting," INISCOM, vol. 444, 2022.

[10] G.-H. Nguyen, A.-N. Nguyen, H.-H. Le, T.-D. Do, "Energy Harvesting and Computation Offloading for UAV-Assisted MEC with NOMA in IoT Network," J. Comm. and Int. Systems, vol. 3, pp. 381, 2023.

[11] X. Zhang, J. Zhang, J. Xiong, L. Zhou, and J. Wei, "Energy-Efficient Multi-UAV-Enabled Multiaccess Edge Computing Incorporating NOMA," IEEE Int. of Things J., vol. 7, no. 6, pp 5613-5627, 2021.

[12] Ishan B., Neeraj K., Sudhanshu T., and Sudeep T., "Energy Consumption Minimization Scheme for NOMA-Based Mobile Edge Computation Networks Underlaying UAV," IEEE Systems Journal, vol. 15, no. 4, pp 5724-5733, 2021.

[13] A.-N. Nguyen, D.-B. Ha, T.-V. Truong, S. Sanguanpong, and C. So-In, "Secrecy Performance Analysis and Optimization for UAV-Relay-Enabled WPT and Cooperative NOMA MEC in IoT Networks," IEEE Access, pp. 127800-127816, 2023.

[14] K. Dogbe, and N. Hakem, "Analysis of full-duplex AF Relaying under Imperfect Channel State Information," USNC-URSI Radio Science Meeting, 2019.

[15] A.-N. Nguyen, and N.-A. Bui, "Performance Analysis of IoT Mobile Edge Computing Networks Using a DF/AF UAV-Enabled Relay with Downlink NOMA," ISIEA, 2023.

[16] I. Gradshteyn and I. Ryzhik, Table of Integrals, Series, and Products. New York: Academic Press (Editor: A Jeffrey and D Zwillinger), 2014.

[17] K. L. Judd, "Quadrature Methods," University of Chicago's Initiative for Computational Economics (ICE).